12^{th} International Conference on Fracture Mechanics of Concrete and Concrete Structures
FraMCoS-12
B.L.A. Pichler, Ch. Hellmich, P. Preinstorfer (Eds)

https://doi.org/10.21012/FC12.1164
MS04:2

ROLE OF THE WEAK INTERFACE ON TOUGHENING IN LAYERED BRITTLE MATERIALS: A COUPLED PHASE FIELD-COHESIVE ZONE MODEL APPROACH TO FRACTURE

Aimane Najmeddine* **and Reza Moini***

* Princeton University
59 Olden Str., Princeton NJ, USA
e-mails: an3801@princeton.edu, rez.moini@princeton.edu

Key words: Brittle fracture, composite, interface, phase-field, CZM, deflection, penetration

Abstract. Interfacial properties in layered microstructures such as composites, rocks, and 3D-printed brittle materials play a significant role in bulk fracture and failure mechanisms, and are critical for the purposeful design of toughening mechanisms in architected materials. Capturing the role of the interface in crack propagation of layered materials is challenging due to the need to incorporate interface elements within the bulk while accounting for bulk fracture. A coupled phase-field and CZM framework, previously developed by authors for crack impinging on an interface, was used to numerically examine the significance of including vs. excluding the weak interface for accurate prediction of crack propagation in layered and functionally graded materials. The crack penetration and deflection scenarios were examined and compared with LEFM theory for a crack tip present in the bulk. It was found that the framework accurately captures the fracture and crack-interface interaction when the crack is present in the bulk, while exclusion of the interface led to inaccurate fracture response. Interfacial failure (i.e., debonding) in the case of crack deflection provides significant energy dissipation (toughness) —17 times greater compared to penetration and 4 times greater compared to the case where the interface is excluded. These dissipative mechanisms from crack-interface interaction can help engineer tougher layered composites. A strategically engineered weak interface can effectively redirect crack propagation, transforming a catastrophic penetration failure into a more controlled deflection mechanism.

1 INTRODUCTION

Layered similar or dissimilar composites (e.g., functionally graded) with interfaces are prevalent in both natural and engineering materials, from rocks to layered concrete structures such as 3D-printed or repaired elements [1, 2]. These materials contain microstructures with layered interfaces that introduce competing cracking phenomena: crack deflection into the interface versus penetration into the bulk [3] (Fig. 1a). The overall fracture response and cracking mechanisms are fundamentally determined by the relative properties of the interface and bulk materials, which govern this competition [4, 5]. Understanding and controlling these mechanisms is critical for the purposeful engineering of toughening mechanisms in architected materials [6–8].

Capturing the role of interfaces in layered materials presents significant numerical challenges, particularly in incorporating interface elements within the bulk while simultaneously accounting for bulk fracture [9]. Various numerical approaches have been developed to better understand fracture in layered materials, including phase-field methods [10–12] and cohe-

sive zone model (CZM) approaches [13–16]. However, using either phase-field or CZM alone has limitations: phase-field methods struggle to represent interfaces effectively, while CZM approaches lack the ability to readily represent fracture with a field quantity that specifically represents damage and its gradient [17, 18].

To address these limitations, several researchers have established coupled phase-field and CZM approaches to fracture [17, 19, 20]. In an earlier work, the authors developed a comprehensive numerical framework capable of handling both elastic and hyperelastic constitutive relationships to understand fracture phenomena in hard-soft architected multi-materials [9]. This framework addresses limitations in simulating interface fracture within a physics-based formulation and leverages the advantages of the potential-based CZM developed by Park, Paulino, and Roesler [21]. While the framework was validated with Linear Elastic Fracture Mechanics (LEFM) (Fig. 1b) for crack impinging on an interface, real natural or engineering materials often contain bulk defects or are examined for fracture properties with a notch present within the bulk. Here, we propose using the previously developed framework to examine fracture in layered materials with an interface for a pre-existing crack (notch) present in the bulk (in the first layer). We assess the utility of the framework and the role of the interface by comparing simulations with and without the interface against LEFM-predicted responses.

2 LEFM Conditions for Crack Propagation in Bi-Layer Systems

Understanding crack propagation in bi-layer composites with *weak* interfaces requires first establishing the conditions under which LEFM theory applies. A critical factor in this assessment is the interface process zone, characterized by its size, l_{pz}, relative to the pre-existing notch length L [15, 17]. This relative process zone size, also known as the fracture-length scale [16], is defined as $\frac{l_{pz}}{L} = \frac{G_c^{\text{int}} E}{\sigma_c^2 L}$ where G_c^{int} is the interface fracture energy, E is the bulk material's Young's modulus, and σ_c is the interface cohesive strength. LEFM theory applies when this ratio approaches zero ($l_{pz}/L \to 0$), indicating a *weak* interface [16, 17]. For interfaces with larger relative process zones, the interaction between crack deflection and penetration becomes more complex and cannot be predicted by LEFM [17]. This work focuses on material assemblies with weak interfaces, where the relative process zone size is negligible.

For a crack impinging on an interface between two materials (Fig. 1b), the competition between crack deflection and penetration depends on two key parameters [4]: (1) the ratio of interface to bulk fracture energy, $G_c^{\text{int}}/G_c^{bulk}$, and (2) Dundur's elastic mismatch parameter, α, defined as: $\alpha = \frac{E_B^* - E_A^*}{E_B^* + E_A^*}$ where E_i^* is the plane strain Young's modulus of material i. When the interface is significantly weaker than the bulk ($G_c^{\text{int}} \ll G_c^{bulk}$), crack deflection dominates. Conversely, higher interface toughness promotes crack penetration. This theoretical criterion is used to investigate the competition between crack penetration and crack deflection through the recently developed coupled phase-field PPR CZM framework [9].

3 Variational Framework for Crack Propagation in Layered Structures

A variational formulation for modeling crack propagation in layered assemblies composed of hard constituents separated by interfacial zones was recently developed by the authors [9]. The key lines are recalled herein. The framework considers a solid body Ω_0 divided into two regions (Ω_0^1 and Ω_0^2) by an interface Γ_0, with each region potentially having different constitutive properties (Fig. 2a).

The kinematics involve a motion mapping $\mathbf{x} = \chi(\mathbf{X}, t)$ from the reference to current configuration (Fig. 2a), with the displacement field defined as $\mathbf{u}(\mathbf{X}, \mathbf{t}) = \mathbf{x} - \mathbf{X}$. The body is subject to body forces $\mathbf{b}_0$ and boundary conditions including applied tractions $\mathbf{t}_0$ and prescribed displacements $\bar{\mathbf{u}}$.

The total potential energy of the layered system with interfaces is composed of three com-

(a) Fracture behavior in monolithic vs multi-layered composites

(b) Crack propagation mechanisms at interfaces according to LEFM theory

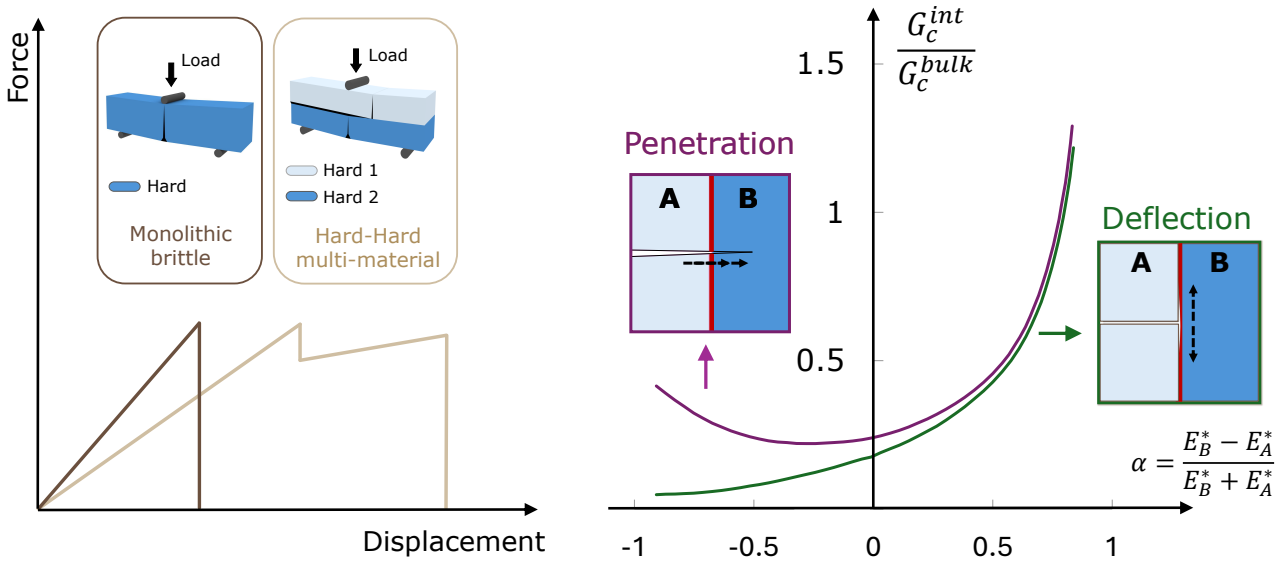

Figure 1: Fracture behavior in layered multi-material composites.

ponents:

$$\Pi(\mathbf{u}, d) = \Pi^{b^k}(\mathbf{u}, d) + \Pi^{\text{int}}(\mathbf{u}) + \mathcal{P}(\mathbf{u}) \quad (1)$$

where Π^{b^k} represents the bulk energy contributions where k refers to the number of layers (i.e., material bulk regions) considered, Π^{int} accounts for interface energy, and $\mathcal{P}$ represents external work.

The bulk contribution incorporates both the strain energy and fracture energy:

$$\Pi^{b^k}(\mathbf{u}, d) = \int_{\Omega_0^k} \Psi^k(\mathbf{F}, d)\mathrm{dV} + \int_{\mathcal{Q}_0} G_c^k \mathrm{dA} \quad (2)$$

where $\Psi^k(\mathbf{F}, d)$ and G_c^k are the Helmholtz free energy and the fracture toughness of bulk material k, respectively, and $\int_{\mathcal{Q}_0} G_c^k \mathrm{dA}$ denotes the energy dissipated due to fracture phenomena at the sharp crack $\mathcal{Q}_0$.

The interface contribution is characterized by a cohesive potential function φ^{int}:

$$\Pi^{\text{int}}(\Delta\mathbf{u}) = \int_{\Gamma_0} \varphi^{\text{int}}(\Delta\mathbf{u})\mathrm{dA} \quad (3)$$

where $\Delta\mathbf{u}$ represents the displacement jump across the interface.

The equilibrium of the system is determined through the principle of stationary energy, requiring that the variation of the total potential energy vanishes:

$$\delta\Pi = \delta\Pi^{b^k} + \delta\Pi^{\text{int}} + \delta\mathcal{P} = 0 \quad (4)$$

3.1 Bulk Material Damage

Rather than modeling the sharp crack $\mathcal{Q}_0$, the phase-field approach to fracture employs a damage field $d(\mathbf{X}, t)$ that varies continuously from 0 (intact material) to 1 (complete fracture) over a localized band $\mathcal{B}$ (Fig. 2b). As such, the energy contribution from $\mathcal{Q}_0$ is regularized through a volumetric approximation of the integral evaluation as follows [23]:

$$\int_{\mathcal{Q}_0} G_c^k \mathrm{dA} \approx \int_{\Omega_0^k} G_c^k \gamma_{(d,\nabla d)} \mathrm{dV} \quad (5)$$

with the crack surface density function:

$$\gamma_{(d,\nabla d)} = \frac{1}{c_\phi}\left[\frac{1}{l_c^k}\phi(d) + l_c^k \nabla d \cdot \nabla d\right] \quad (6)$$

where $c_\phi = 4\int_0^1 \sqrt{\phi(y)}\mathrm{d}y$, and $\phi(d) = d^2$ is a quadratic crack geometric function (AT2 formulation). The length scale parameter l_c^k controls the diffuse damage band width, with Griffith theory recovered as $l_c^k \to 0$.

(a) Initial to current configuration

(b) Sharp to diffuse crack topology

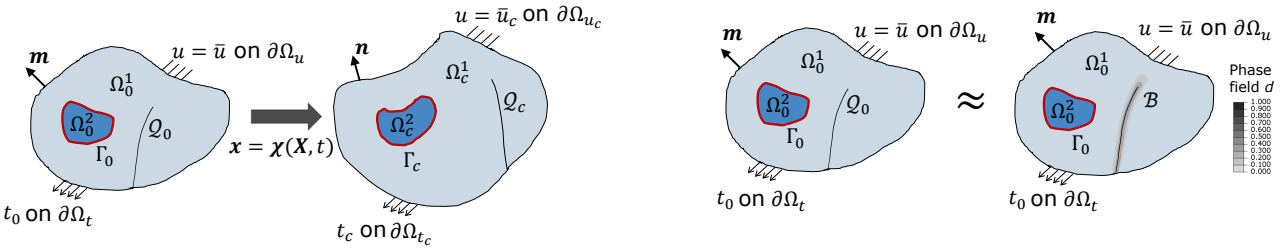

Figure 2: (a) Kinematics of a solid body containing an initial crack $\mathcal{Q}_0$ and an interface Γ_0 separating two regions Ω_0^1 and Ω_0^2 in the initial and Ω_c^1 and Ω_c^2 in the current configurations. (b) Substitution of the sharp crack topology $\mathcal{Q}_0$ with a diffuse representation $\mathcal{B}$ having a finite width over which a scalar phase-field variable varies from 0 (intact) to 1 (fractured).

The complete bulk contribution (Eq. 2) becomes:

$$\begin{aligned}\Pi^{b^k}(\mathbf{u},d) = &\int_{\Omega_0^k} \Psi^k(\mathbf{F},d)\mathrm{dV} \\ &+ \int_{\Omega_0^k} G_c^k \gamma_{(d,\nabla d)}\mathrm{dV}\end{aligned} \tag{7}$$

from which, the following variational expressions with respect to displacement and phase-field are obtained:

$$\begin{aligned}\delta\Pi_u^{b^k} &= \int_{\Omega_0^k} \frac{\partial\Psi^k(\mathbf{F},d)}{\partial\mathbf{F}}\frac{\partial\delta\mathbf{u}}{\partial\mathbf{X}}\mathrm{dV} \\ \delta\Pi_d^{b^k} &= \int_{\Omega_0^k} \frac{\partial\Psi^k(\mathbf{F},d)}{\partial d}\delta d\mathrm{dV} \\ &+ \int_{\Omega_0^k} \frac{G_c^k}{c_\phi l_c}\phi'_{(d)}\delta d\mathrm{dV} \\ &- \int_{\Omega_0^k} \frac{2G_c^k l_c}{c_\phi}\Delta d\delta d\mathrm{dV}\end{aligned} \tag{8}$$

where $\Delta d = \nabla\cdot\nabla d$ is the Laplacian of the phase-field variable.

3.2 Interface Dissipation

To account for the interface contribution to overall energy potential, a displacement jump $\Delta\mathbf{u}$ is defined across the interfacial region Γ_0, with tangential and normal components: $\Delta\mathbf{u} = (\Delta\mathbf{u}_t, \Delta\mathbf{u}_n)^\mathsf{T}$. The interface potential energy is then written in terms of the displacement jump as:

$$\Pi^{\mathrm{int}}(\Delta\mathbf{u}) = \int_{\Gamma_0} \varphi^{\mathrm{int}}(\Delta\mathbf{u})\mathrm{dA} \tag{9}$$

The interface variation therefore takes the form:

$$\delta\Pi^{\mathrm{int}} = \delta\mathbf{u}^\mathsf{T}\int_{\Gamma_0}\left(\frac{\partial\Delta\mathbf{u}}{\partial\mathbf{u}}\right)^\mathsf{T}\mathbf{T}\mathrm{dA} \tag{10}$$

where $\mathbf{T}$ is the first Piola-Kirchhoff cohesive traction vector, obtained as:

$$\mathbf{T} = \frac{\partial\varphi^{\mathrm{int}}(\Delta\mathbf{u})}{\partial\Delta\mathbf{u}} = (T_t, T_n)^\mathsf{T} \tag{11}$$

4 Constitutive Relationships

This section presents the constitutive relationships corresponding to the bulk and interface components of the coupled phase-field CZM framework [9] .

4.1 Bulk

The constitutive behavior of the bulk is characterized as a linear elastic material through the following intact Helmholtz free-energy:

$$\psi(\mathbf{F}) = \frac{1}{2}\mathbf{E}:\mathbb{C}:\mathbf{E} \tag{12}$$

where $\mathbf{E}$ is the Green-Lagrange strain tensor and $\mathbb{C}$ is the elastic stiffness tensor. To capture different behaviors under tension and compression, the deformation gradient is decomposed into volumetric and isochoric parts:

$$\begin{cases}\mathbf{F}_{iso} = (\det\mathbf{F})^{-1/3}\mathbf{F} \\ \mathbf{F}_{vol} = (\det\mathbf{F})^{1/3}\mathbf{I}\end{cases} \tag{13}$$

The strain tensor is similarly decomposed:

$$\begin{cases} \mathbf{E}_{iso} = \frac{1}{2}(\mathbf{F}_{iso}^{\mathsf{T}}\mathbf{F}_{iso} - \mathbf{I}) \\ \mathbf{E}_{vol} = \frac{1}{2}(\mathbf{F}_{vol}^{\mathsf{T}}\mathbf{F}_{vol} - \mathbf{I}) \end{cases} \tag{14}$$

The degraded elastic strain tensor incorporates damage through:

$$\tilde{\mathbf{E}}_{(d)} = \begin{cases} (1-d)\mathbf{E}, & \text{if } \det \mathbf{F} \geq 1 \\ (1-d)\mathbf{E} + d\mathbf{E}_{vol}, & \text{otherwise} \end{cases} \tag{15}$$

This formulation ensures that damage only affects the volumetric component under dilation and effectively handles tension-compression asymmetry [24]. The final degraded Helmholtz free energy function is:

$$\Psi_{(\mathbf{F},d)} = \frac{1}{2}\tilde{\mathbf{E}}_{(d)} : \mathbb{C} : \tilde{\mathbf{E}}_{(d)} \tag{16}$$

The first Piola-Kirchhoff stress tensor is then derived as $\mathbf{P} = \frac{\partial \Psi}{\partial \mathbf{F}}$.

4.2 Interface

The detailed constitutive description of the interface is provided in [9]; we recall the key aspects herein. The interface behavior is modeled using the Park-Paulino-Roesler (PPR) potential-based cohesive zone model [21, 22], which offers advantages over traditional approaches by providing consistent work-of-separation and physically meaningful fracture parameters. The PPR potential is expressed as:

$$\begin{aligned} \varphi^{\text{int}} = & \min(\mathcal{G}_n, \mathcal{G}_t) + \\ & \left[\Gamma_n \left(1 - \frac{\Delta \mathbf{u}_n}{\delta_n}\right)^r \left(\frac{m}{r} + \frac{\Delta \mathbf{u}_n}{\delta_n}\right)^m + \right. \\ & \left. \langle \mathcal{G}_n - \mathcal{G}_t \rangle \right] \times \\ & \left[\Gamma_t \left(1 - \frac{|\Delta \mathbf{u}_t|}{\delta_t}\right)^s \left(\frac{n}{s} + \frac{|\Delta \mathbf{u}_t|}{\delta_t}\right)^n + \right. \\ & \left. \langle \mathcal{G}_t - \mathcal{G}_n \rangle \right] \end{aligned} \tag{17}$$

where $\mathcal{G}_n$, $\mathcal{G}_t$ are Mode-I and Mode-II fracture energies, and Γ_n, Γ_t are energy constants [21]. Furthermore, m and n are exponents of the PPR CZM model.

The normal and tangential tractions are derived from this potential:

$$\begin{aligned} T_n = & \frac{\Gamma_n}{\delta_n} \left[m \left(1 - \frac{\Delta \mathbf{u}_n}{\delta_n}\right)^r \left(\frac{m}{r} + \frac{\Delta \mathbf{u}_n}{\delta_n}\right)^{m-1} - \right. \\ & \left. r \left(1 - \frac{\Delta \mathbf{u}_n}{\delta_n}\right)^{r-1} \left(\frac{m}{r} + \frac{\Delta \mathbf{u}_n}{\delta_n}\right)^m \right] \times \\ & \left[\Gamma_t \left(1 - \frac{|\Delta \mathbf{u}_t|}{\delta_t}\right)^s \left(\frac{n}{s} + \frac{|\Delta \mathbf{u}_t|}{\delta_t}\right)^n + \right. \\ & \left. \langle \mathcal{G}_t - \mathcal{G}_n \rangle \right] \end{aligned} \tag{18}$$

$$\begin{aligned} T_t = & \frac{\Gamma_t}{\delta_t} \left[n \left(1 - \frac{|\Delta \mathbf{u}_t|}{\delta_t}\right)^s \left(\frac{n}{s} + \frac{|\Delta \mathbf{u}_t|}{\delta_t}\right)^{n-1} - \right. \\ & \left. s \left(1 - \frac{|\Delta \mathbf{u}_t|}{\delta_t}\right)^{s-1} \left(\frac{n}{s} + \frac{|\Delta \mathbf{u}_t|}{\delta_t}\right)^n \right] \times \\ & \left[\Gamma_n \left(1 - \frac{\Delta \mathbf{u}_n}{\delta_n}\right)^r \left(\frac{m}{r} + \frac{\Delta \mathbf{u}_n}{\delta_n}\right)^m + \right. \\ & \left. \langle \mathcal{G}_n - \mathcal{G}_t \rangle \right] \frac{\Delta \mathbf{u}_t}{|\Delta \mathbf{u}_t|} \end{aligned} \tag{19}$$

where r and s are shape parameters that control the softening behavior: $r, s < 2$ produces concave traction-separation curves, while $r, s \gg 2$ yields convex curves typical of quasi-brittle materials. δ_n and δ_t are the final crack openings in the normal and tangential directions, respectively [21].

The constitutive relationships described for the bulk and interface components have been incorporated into the finite element (FE) software ABAQUS/Standard [25] through the utilization of a user-defined element subroutine (UEL) [9]. In particular, user-defined elements have been developed for four-node isoparametric quadrilateral plane-strain elements for the material bulk, and zero-thickness elements for the interface.

5 Numerical simulations

The capability of the coupled phase-field PPR framework [9] to numerically simulate the crack propagation mechanisms in layered hard-hard composites is evaluated and compared

Table 1: Material and interface properties used in the hard-hard bi-layer composite

	Bulk					Interface			
		E (GPa)	ν	G_c (N/mm)	l_c (mm)	$\mathcal{G}_n$ (N/mm)	$\mathcal{G}_t$ (N/mm)	σ_{max} (MPa)	τ_{max} (MPa)
Set (i)	Material A	70	0.3	0.05	0.005	0.05	0.05	170	170
	Material B	210	0.3	0.05	0.005				
Set (ii)	Material A	70	0.3	0.05	0.005	0.01	0.01	170	170
	Material B	210	0.3	0.05	0.005				

against the LEFM theory from Section 2. The analysis is carried out by examining how the framework captures the competition between crack deflection and penetration in bi-layered hard-hard composites containing weak interfaces and a notch within the bulk first layer. Furthermore, the importance of incorporating the CZM component within the overall framework to simulate the correct crack propagation mechanism in such composites as predicted by LEFM theory is demonstrated.

5.1 Deflection vs. Penetration

The case of a two-dimensional (2D) bi-layer hard-hard composite separated by an interface is considered, containing a pre-existing notch (i.e., initial crack) in Material A behind an interface and loaded under direct tension, as shown in Fig. 3a. The general case of a composite comprising two dissimilar materials with varying constitutive properties is considered.

A 1×1 mm^2 bi-layer single-edge notch configuration is analyzed, consisting of two layers of hard materials with distinct properties, separated by an interfacial boundary. Here, the notch in the first layer (i.e., Material A), unlike the conventional case of a crack impinging on an interface, extends only through half the width of the left layer (0.25 mm in length), as depicted in Fig. 3a. The composite is subjected to uniform tensile loading via prescribed displacement along both the top and bottom edges of the domain. For the bulk materials, plane-strain four-node quadrilateral elements are implemented (Fig. 3a), which incorporate the constitutive relationships detailed in Section 4. The interface between the two material layers is modeled using zero-thickness cohesive elements (Fig. 3a), governed by the PPR constitutive relationships described in Section 3.2. In this implementation, both initial slope indicators l_n and l_t are set to 0.015, while the shape parameters r and s are assigned the value of 2. To ensure accurate crack profiles as well as mesh-convergent solutions, local mesh refinement was used in the vicinity of the interface and in regions where bulk fracture is anticipated. In particular, the mesh size in these critical regions was set to 0.0025 mm, i.e., half the phase-field characteristic length scale reported in Table 1.

Two distinct sets of material and interface constitutive properties is investigated, specifically selected to demonstrate different crack propagation mechanisms as predicted by LEFM theory [4]. Set (i) is configured to promote crack penetration, while set (ii) is chosen to advance crack deflection. The two property sets are plotted on the He-Hutchinson diagram (Fig. 3b). The complete material and interface properties for both sets are detailed in Table 1.

The numerical simulations using set (i), yield results that align with LEFM predictions, as demonstrated by the phase-field and vertical displacement contours shown in Fig. 3c. Upon reaching the critical displacement threshold, the crack initiates at the tip of the pre-existing notch, propagates through the first layer (i.e., Material A), then penetrates the interface and continues propagating into Material B, ultimately resulting in complete fracture along the bi-layer center-line. This penetrative failure mechanism, while successfully predicted by the numerical framework, can be an undesirable

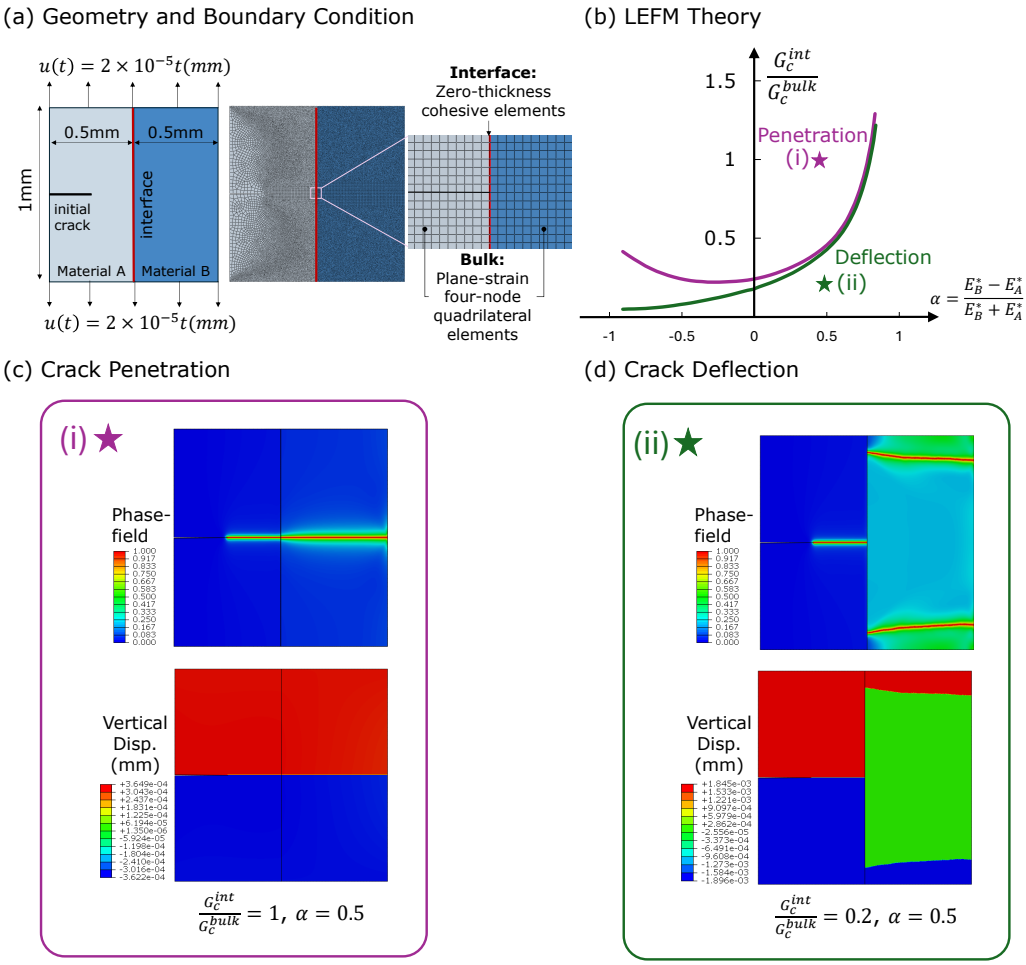

Figure 3: (a) Geometry, boundary conditions, and FE mesh for a plane-strain bi-layer hard-hard single-edge notch composite containing an interface loaded by a prescribed displacement in tension, (b) locations of the theoretically expected crack propagation mechanism for the two sets of material properties selected, (c) and (d) computationally simulated phase-field and vertical displacement contours at the end of the simulation for the case of crack penetration and deflection, respectively, viewed on the undeformed configuration.

mechanism in composite material design. Such direct through-material failure occurs abruptly, bypassing potential interface interactions that could otherwise enhance the composite's load-bearing capacity through more gradual energy dissipation along the interface, preventing brittle fracture.

Similarly, the simulations using set (ii) demonstrate agreement with LEFM theoretical predictions, exhibiting the anticipated crack deflection mechanism. Fig. 3d illustrates this behavior, which aligns with the predictions shown in the He-Hutchinson plot (Fig. 3b). The crack initiates at the pre-existing notch and propagates through Material A; however, unlike in the penetration case, rather than penetrating through Material B, the crack deflects in two directions along the interface, travels along the depth of the domain, and finally kinks symmetrically into Material B at a relatively distant location away from the center (near the upper and lower edges of the composite). Notably, while crack deflection is the primary mechanism, the complete crack propagation path reveals a subsequent penetration through Material B at a later stage in the loading process. This delayed penetration occurs only after significant interfacial deflection has taken place, as evi-

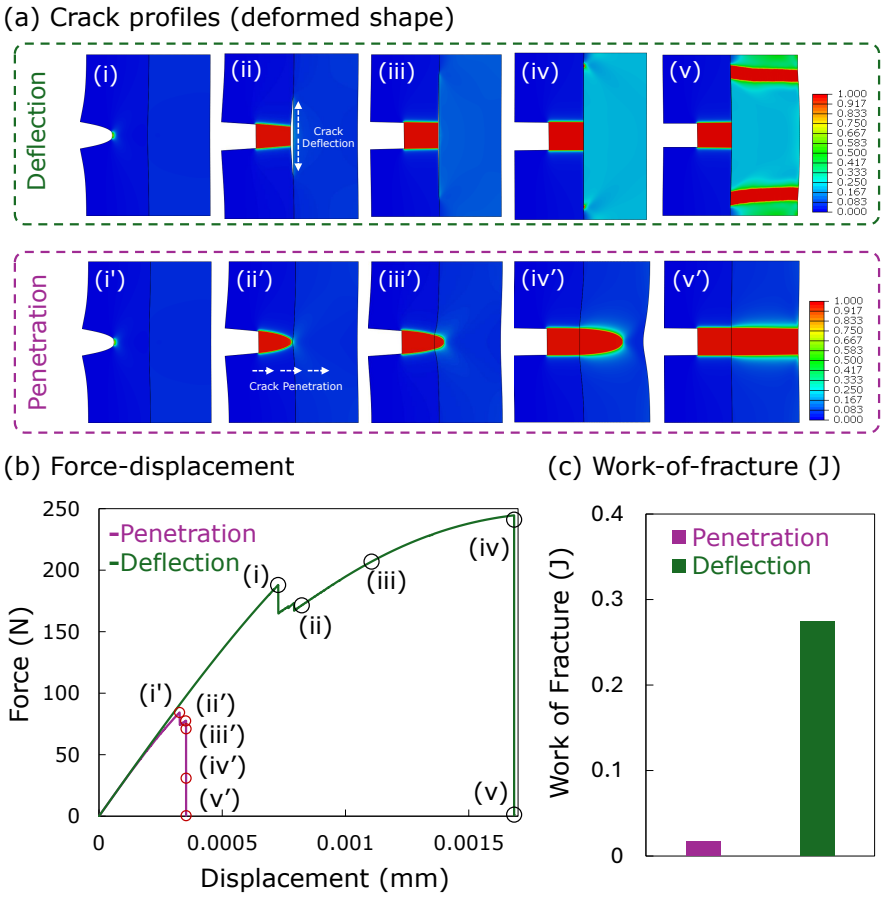

Figure 4: Comparison of the crack propagation process (viewed on the deformed configuration) and the force-displacement curves corresponding to the two mechanisms of fracture investigated in the bi-layer hard-hard composite, i.e., crack deflection and crack penetration.

denced by the phase-field contours in Fig. 3d. The delay in complete fracture represents a significant advantage from the perspective of the design of failure modes, as the interfacial deflection and associated energy dissipation along the interface effectively postpone catastrophic failure. This behavior is in contrast with the immediate penetration observed for set (i), highlighting how purposeful material and interface property selection can enhance the composite's overall fracture resistance through controlled crack path modification and energy dissipation mechanisms. Note that the deflection mechanism observed results in sliding of the upper and lower left blocks with respect to their rightward counterpart as evidenced by the discontinuous vertical displacement field shown in Fig. 3d.

The force-displacement response reveals a distinct contrast between crack penetration and deflection mechanisms, as illustrated in Fig. 4b. The deflection case demonstrates superior mechanical performance, achieving both higher peak loads and greater displacement before final failure compared to the penetration case. This improved performance manifests in the work-of-fracture (Fig. 4c), calculated from the area under the force-displacement curves. Specifically, the deflection mechanism generates a work-of-fracture of $0.27\ J$, approximately 17 times greater than the $0.0165\ J$ observed in the penetration case. When normalized by the fractured surface area, this difference translates to a 6-fold increase in fracture toughness, with values of $0.13\ J$ and $0.022\ J$ for the deflection and penetration cases, respectively.

Note that the process of crack penetration and deflection described above can be further visualized through the phase-field evolu-

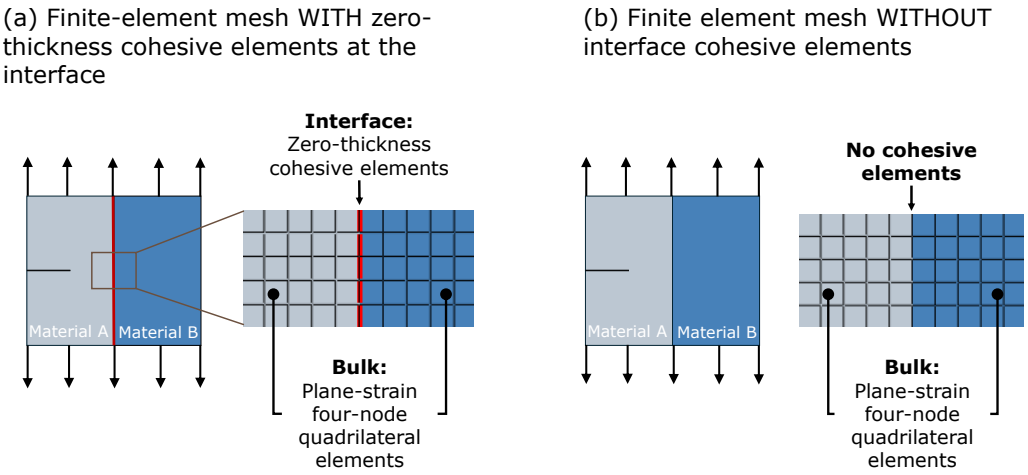

Figure 5: FE mesh corresponding for the case when (a) zero-thickness cohesive elements were implemented at the interface and assigned PPR CZM constitutive properties, and (b) the interface was not simulated and therefore no cohesive elements were implemented at the inter-layer boundary between the two material blocks.

tion shown in Fig. 4a, which illustrates the detailed progression of both fracture mechanisms through stages i-v and i'-iv' for the deflection and penetration cases, respectively.

The distinct mechanical responses observed for penetration and deflection underscore the critical role of interfacial properties in the design of layered brittle composites. A strategically engineered weak interface can effectively redirect crack propagation, transforming a catastrophic penetration failure into a more controlled deflection mechanism. This behavioral modification not only enhances the composite's load-bearing capacity but also significantly improves its overall fracture toughness through progressive, rather than catastrophic, failure.

5.2 Significance of incorporating CZM constitutive relationships

To further demonstrate the importance of incorporating the interfacial constitutive relationships (i.e., PPR CZM) into the coupled framework, the previous crack deflection case is revisited (set (ii) in Table 1) and a comparative analysis is conducted by removing the cohesive interface elements while maintaining all other parameters constant. In the case for which the cohesive interface elements were not included, the FE mesh simply did not contain zero-thickness cohesive elements at the inter-layer boundary between the two material blocks. Fig. 5 illustrates the two FE mesh representations.

Fig. 6 compares the phase-field contours, vertical displacement fields, and force-displacement responses obtained for the two cases examined (i.e., *with* zero-thickness cohesive elements assigned PPR CZM constitutive properties, and *without* interface and thus no cohesive elements implemented at the inter-layer boundary). When the cohesive elements are implemented between the two material blocks, the theoretically predicted deflection mechanism is recovered as previously discussed, wherein the crack redirects along the interface before eventual penetration through Material B. This behavior manifests in the force-displacement response through sustained load-bearing capacity and enhanced displacement before final failure.

In contrast, removing the interface cohesive elements fundamentally alters the predicted crack propagation responses. Without the cohesive zone implementation, the crack inaccurately penetrates directly through both materials, bypassing the deflection mechanism entirely and failing to capture the physically expected deflection mechanism from LEFM

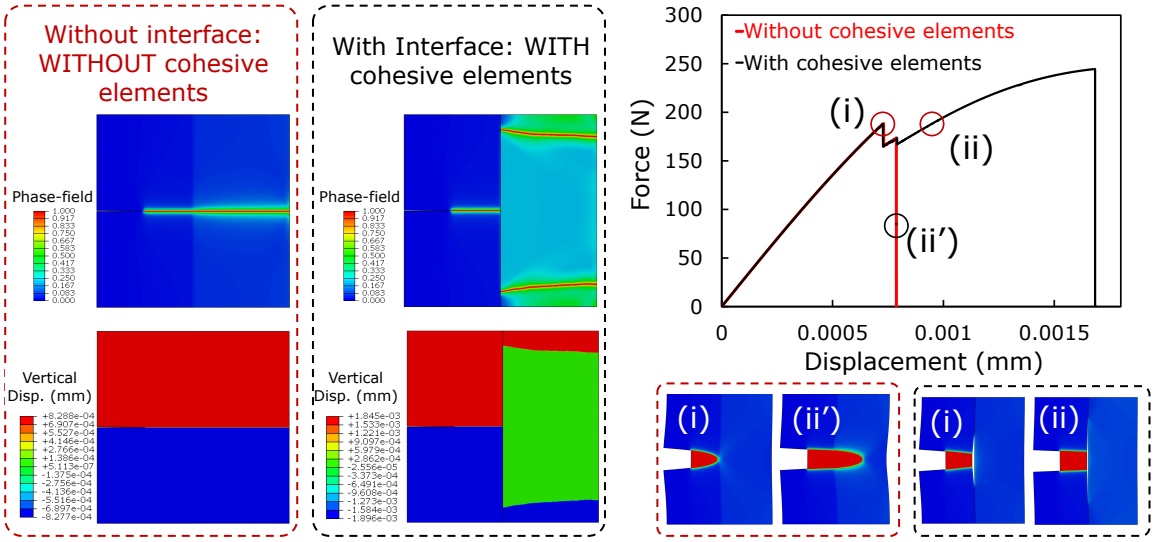

Figure 6: Comparison of the crack profiles and force-displacement curves corresponding to the two cases: when the cohesive elements *were not* implemented (i.e., when the CZM *was not* incorporated) and when the cohesive elements *were* implemented (i.e., when the CZM *was* incorporated). Inaccurate crack propagation is observed for the case when the CZM is not implemented.

(Fig. 3b). This direct penetration results in premature failure at a significantly lower displacement level, as evidenced by the abrupt drop in the force-displacement curve in Fig. 6, fundamentally misrepresenting the composite's actual mechanical behavior. Evidently, the work-of-fracture is underestimated by 4-fold when the cohesive elements are not implemented, further indicating that not incorporating the interfacial constitutive properties leads to inaccurate quantification of energy dissipation and fracture behavior. The phase-field contours clearly illustrate this difference, showing continuous crack propagation through Material B rather than the interfacial deflection and separation observed in the properly simulated case (i.e., the case with proper interface implementation). This penetrative behavior directly contradicts LEFM theoretical predictions for the given material property set (ii), which anticipates crack deflection as shown in Fig. 3b.

The findings underscore that accurate capture of composite failure behavior requires proper implementation of interfacial energy contributions through CZM relationships, as formulated in Eq. 1. This finding has significant implications for computational modeling of composite materials, where interface behavior plays a crucial role in determining overall mechanical performance and failure characteristics.

6 CONCLUSIONS

This work demonstrates the critical importance of properly accounting for the interfacial constitutive relationships in predicting the fracture behavior of brittle hard-hard composite materials such as 3D-printed cementitious materials. Through detailed phase-field simulations incorporating cohesive zone modeling, it is highlighted that crack propagation pathways are significantly influenced by the interplay between bulk material properties and interface characteristics (i.e., crack-interface interaction along the propagation path). The results reveal that strategically designed weak interfaces (i.e., architected interfaces) can effectively redirect crack propagation from potentially catastrophic penetration to more controlled deflection mechanisms, substantially enhancing the composite's load-bearing capacity and energy dissipation capabilities.

The comparative analysis between models with and without interface implementation

clearly demonstrates that omitting the interface not only fails to capture the correct crack propagation mechanism according to LEFM theory, but also significantly underestimates the composite's mechanical performance and energy dissipation capacity. The results underscore the critical necessity of incorporating interfacial energy contributions through proper CZM implementation, and have profound implications for the computational modeling of composite materials, functionally graded materials/interfaces, and 3D-printed brittle/quasi-brittle materials such as concrete, emphasizing that accurate prediction of failure mechanisms requires explicit consideration of interfacial behavior through appropriate constitutive relationships.

7 Appendix

The following supplementary videos have been appended:

- Video 1. Phase-field profile for the crack deflection scenario: https://youtu.be/rhQ0FFl1JKI
- Video 2. Phase-field profile for the crack penetration scenario: https://youtu.be/cV3ahVXW3Ds

8 Acknowledgment

The authors gratefully acknowledge the time and support from the Eric and Wendy Schmidt Transformative Technology Fund Schmidt and the National Science Foundation Advanced Manufacturing Program (2217985).

REFERENCES

[1] Rodriguez, F. B., Moini, R., Agrawal, S., Williams, C. S., Zavattieri, P. D., Olek, J., Youngblood, J. P., and Varma, A. H. (2024). Mechanical response of small-scale 3D-printed steel-mortar composite beams. *Cement and Concrete Composites*, 154:105795.

[2] Gupta, S., Esmaeeli, H. S., Prihar, A., Ghantous, R. M., Weiss, W. J., and Moini, R. (2023). Fracture and transport analysis of heterogeneous 3D-Printed lamellar cementitious materials. *Cement and Concrete Composites*, 140:105034.

[3] Moini, R. 2023. Perspectives in architected infrastructure materials. *RILEM Technical Letters* **8**:125–140.

[4] He, M. Y., and Hutchinson, J. W. 1989. Crack deflection at an interface between dissimilar elastic materials. *International Journal of Solids and Structures* **25**:1053–1067.

[5] Leguillon, D., Lacroix, C., and Martin, E. 2000. Interface debonding ahead of a primary crack. *Journal of the Mechanics and Physics of Solids* **48**:2137–2161.

[6] Prihar, A., Garlock, M. E. M., Najmeddine, A., and Moini, R. 2024. Mechanical performance of sinusoidally architected concrete enabled by robotic additive manufacturing. *Materials & Design* **238**:112671.

[7] Gupta, S., Esmaeeli, H. S., and Moini, R. (2024). Tough and Ductile Architected Nacre-Like Cementitious Composites. *Advanced Functional Materials*, 2313516.

[8] Moini, R., Rodriguez, F., Olek, J., Youngblood, J. P., and Zavattieri, P. D. (2024). Mechanical properties and fracture phenomena in 3D-printed helical cementitious architected materials under compression. *Materials and Structures*, 57(7):170.

[9] Najmeddine, A., Moini, R., and Gupta, S. (2024). Coupled large deformation phase-field and cohesive zone model for crack propagation in hard-soft multi-materials. *Journal of the Mechanics and Physics of Solids*, (in press).

[10] Kumar, A., Bourdin, B., Francfort, G. A., and Lopez-Pamies, O. 2020. Revisiting nucleation in the phase-field approach to

brittle fracture. *Journal of the Mechanics and Physics of Solids* **142**:104027.

[11] Najmeddine, A., and Shakiba, M. 2023. Physics and chemistry-based phase-field constitutive framework for thermo-chemically aged elastomer. *International Journal of Mechanical Sciences* pp. 108721.

[12] Najmeddine, A., and Shakiba, M. 2024. Efficient BFGS quasi-Newton method for large deformation phase-field modeling of fracture in hyperelastic materials. *Engineering Fracture Mechanics* **310**:110463.

[13] Needleman, A. 1990. An analysis of decohesion along an imperfect interface. *International Journal of Fracture* **42**:21–40.

[14] Tvergaard, V., and Hutchinson, J. W. 1992. The relation between crack growth resistance and fracture process parameters in elastic-plastic solids. *Journal of the Mechanics and Physics of Solids* **40**:1377–1397.

[15] Espinosa, H. D., and Zavattieri, P. D. 2003. A grain level model for the study of failure initiation and evolution in polycrystalline brittle materials. Part I: Theory and numerical implementation. *Mechanics of Materials* **35**:333–364.

[16] Parmigiani, J. P., and Thouless, M. D. 2006. The roles of toughness and cohesive strength on crack deflection at interfaces. *Journal of the Mechanics and Physics of Solids* **54**:266–287.

[17] Paggi, M., and Reinoso, J. 2017. Revisiting the problem of a crack impinging on an interface: a modeling framework for the interaction between the phase field approach for brittle fracture and the interface cohesive zone model. *Computer Methods in Applied Mechanics and Engineering* **321**:145–172.

[18] Marulli, M. R., Valverde-González, A., Quintanas-Corominas, A., Paggi, M., and Reinoso, J. 2022. A combined phase-field and cohesive zone model approach for crack propagation in layered structures made of nonlinear rubber-like materials. *Computer Methods in Applied Mechanics and Engineering* **395**:115007.

[19] Carollo, V., Reinoso, J., and Paggi, M. 2018. Modeling complex crack paths in ceramic laminates: A novel variational framework combining the phase field method of fracture and the cohesive zone model. *Journal of the European Ceramic Society* **38**:2994–3003.

[20] Hansen-Dörr, A. C., Dammaß, F., de Borst, R., and Kästner, M. 2020. Phase-field modeling of crack branching and deflection in heterogeneous media. *Engineering Fracture Mechanics* **232**:107004.

[21] Park, K., Paulino, G. H., and Roesler, J. R. 2009. A unified potential-based cohesive model of mixed-mode fracture. *Journal of the Mechanics and Physics of Solids* **57**:891–908.

[22] Park, K., and Paulino, G. H. 2011. Cohesive zone models: a critical review of traction-separation relationships across fracture surfaces. *Applied Mechanics Reviews* **64**:060802.

[23] Miehe, C., Hofacker, M., and Welschinger, F. 2010. A phase field model for rate-independent crack propagation: Robust algorithmic implementation based on operator splits. *Computer Methods in Applied Mechanics and Engineering* **199**(45-48):2765-2778.

[24] Shahba, A., and Ghosh, S. 2019. Coupled phase field finite element model for crack propagation in elastic polycrystalline microstructures. *International Journal of Fracture* **219**:31-64.

[25] SIMULIA. 2014. Abaqus 6.14 Documentation. Dassault Systèmes, Providence, RI, USA.